Environ. Sci. Technol. **2004**, *38,* 2232−2241

Simultaneous Prediction of *Cryptosporidium parvum* Oocyst Inactivation and Bromate Formation during Ozonation of Synthetic Waters

JAE-HONG KIM,[†] URS VON GUNTEN,[‡] AND BENITO J. MARIÑAS*,[§]

School of Civil and Environmental Engineering, Georgia Institute of Technology, Atlanta, Georgia 30332-0512, Swiss Federal Institute for Environmental Science and Technology (EAWAG), Ueberlandstrasse 133, CH-8600, Dübendorf, Switzerland, and Department of Civil and Environmental Engineering, University of Illinois at Urbana−Champaign, Urbana, Illinois 61801

A model was developed to simultaneously assess *Cryptosporidium parvum* oocyst inactivation and bromate formation during ozonation of synthetic solutions in batch and flow-through reactors. The model incorporated 65 elementary chemical reactions involved in the decomposition of ozone and the oxidation of bromine species and their corresponding rate or equilibrium constants reported in the literature. Ozonation experiments were performed with a laboratory-scale batch reactor to evaluate the model with respect to the rate of ozone decomposition and bromate formation. The model was found to provide a good representation of experimental results when the ozone decomposition initiation reaction with hydroxide ion was assumed to produce superoxide radical instead of the alternatively proposed product hydrogen peroxide. The model was further developed to simulate the performance of a flow-through bubble-diffuser reactor with an external recirculation line. Each compartment of the reactor (bubble column and recirculation line) was assumed to behave as a plug flow reactor as supported by tracer test results, and an empirical correlation was used to represent the rate of ozone gas transfer in the bubble column. Model predictions of the performance of the flow-through ozone bubble-diffuser contactor were in good agreement with experimental results obtained for bromate formation and *C. parvum* oocyst inactivation under all conditions investigated. Additional model simulations revealed that hydrodynamic conditions had a more pronounced effect on *C. parvum* oocyst inactivation than on bromate formation. In contrast, pH had a strong effect on bromate formation without affecting the inactivation efficiency of *C. parvum* oocysts for a given level of exposure to ozone. These findings suggested that bromate formation could be minimized while achieving target inactivation levels for *C. parvum* oocysts by designing ozone reactors with hydrodynamic conditions approaching that of an ideal plug flow reactor and by lowering the pH of the target water.

* Corresponding author telephone: (217)333-6961; fax: (217)333-6968; e-mail: marinas@uiuc.edu.

[†] Georgia Institute of Technology.

[‡] EAWAG.

[§] University of Illinois at Urbana−Champaign.

Introduction

The application of ozone as a disinfectant has been gaining popularity because of its effectiveness in treating pathogens such as oocysts of the protozoan parasite *Cryptosporidium parvum* (*1*−*6*), which have shown strong resistance to free chlorine and monochloramine (*3*, *5*−*7*). In addition, due to stringent regulations for trihalomethanes and other halogenated disinfection byproducts (DBPs), ozone has been identified as an effective alternative to free and combined chlorine. However, application of ozone can lead to the generation of other types of halogen-derived DBPs of public health concern (*8*−*10*). The DBP of most concern during ozonation is bromate (BrO_3^-), a potential human carcinogen, which is formed during ozonation of bromide-containing waters and is currently regulated at 10 μg/L in the United States and the European Union (*11*, *12*). Therefore, there is a need for optimizing the ozone disinfection process to provide adequate inactivation of *C. parvum* oocysts with minimum production of bromate. To achieve this goal, the kinetics of both *C. parvum* oocyst inactivation and bromate formation need to be elucidated and incorporated into a predictive model for the ozone disinfection process.

***C. parvum* Inactivation.** The kinetics of *C. parvum* oocyst inactivation with ozone has been studied for more than a decade (*1*−*7*, *13*). Inactivation curves resulting from plotting oocyst survival ratios versus CT (i.e., the product of disinfectant concentration and contact time for a semi-batch reactor or the integral of disinfectant concentration over contact time for a batch reactor) have been characterized by the presence of an initial lag phase during which little inactivation occurs followed by a phase of pseudo-first-order decrease in viability. The extent of the lag phase and the rate of post-lag phase inactivation have been shown to vary between oocyst lots, but for a given lot, the inactivation rate of *C. parvum* oocysts has been found to have a first-order dependence on the overall exposure to ozone (*4*). As a result, the CT required to achieve a certain level of *C. parvum* oocyst inactivation has been found to be independent of the dissolved ozone concentration (*2*−*6*).

Bromate Formation. Bromate is formed from bromide through a complex system of chemical reactions involving not only ozone but also several secondary oxidants such as hydroxyl and carbonate radicals. These secondary oxidants are formed from the decomposition of ozone in water. Accordingly, the kinetics of bromate formation during ozonation is affected by several water quality parameters such as pH, alkalinity, amount and composition of natural organic matter, and temperature (*8*, *14*). Empirical predictive models for bromate formation during ozonation of specific bromide-containing waters have been proposed (*15*, *16*), but their applicability toward a wider range of waters has failed. Accordingly, mechanistic predictive models incorporating elementary chemical reactions involved in bromate formation during ozonation and advanced oxidation processes have been developed (*17*−*20*). An attempt (*20*) has also been made to combine bromate formation with a mechanistic model for ozone decomposition based on Staehelin, Bühler, and Hoigné (*21*, *24*, *25*); Forni et al. (*22*); and Tomiyasu et al. (*23*). In addition, several studies have investigated the effect of chemical species, such as ammonia, hydrogen peroxide, and bicarbonate/carbonate on bromate formation (*19*, *26*−*28*).

10.1021/es034760w CCC: $27.50

Published on Web 02/24/2004

A review on bromate formation during ozonation can be found in ref *29*.

Flow-Through Systems. Several studies have reported the prediction of *C. parvum* oocyst inactivation in flow-through ozone contactors where hydrodynamic conditions play an important role in determining overall process efficiency (*30*−*34*). These studies have demonstrated applicability of hydrodynamic models for accurate prediction of *C. parvum* oocyst inactivation efficiencies in flow-through systems. Similar efforts (*35*−*37*) have been made for bromate formation in flow-through systems but mostly using empirical models due to complexity in mechanistic predictive models when coupled with hydrodynamic models. Moreover, limited effort has been made for simultaneous consideration of *C. parvum* oocyst inactivation and bromate formation in flow-through ozone disinfection systems (*38*).

In the present study, we developed a mathematical model for the simultaneous prediction of *C. parvum* oocyst inactivation and bromate formation in flow-through ozone bubble-diffuser contactors, the most common reactor design currently in use for drinking water disinfection with ozone in the United States (*39*). The model included the following key elements: (i) ozone decomposition mechanism; (ii) bromate formation mechanism; (iii) *C. parvum* oocyst inactivation kinetics; (iv) ozone mass transfer; and (v) contactor hydrodynamics. The mechanistic part of the model was verified in synthetic waters with respect to ozone decomposition and bromate formation. These elements were then integrated into a model that allows simulation of a lab-scale flow-through ozone bubble-diffuser contactor. The model was verified by performing ozonation experiments with synthetic waters spiked with both bromide and *C. parvum* oocysts.

Experimental Section

Materials. All experiments were performed with distilled−deionized (DDI) water and chemicals of reagent or higher grade. The total organic carbon content of DDI water, checked at various times throughout the study, was found to be in the range of 0.05−0.2 mg/L. Suspensions of Iowa strain C. *parvum* oocysts (lots A and B) (propagated in bovine hosts, purified, and suspended in a phosphate buffer solution containing antibiotics and an antimycotic) were obtained from the Department of Veterinary Science, University of Arizona. Upon arrival to the University of Illinois, the oocyst suspensions were cleaned and stored following procedures described previously (*2*).

Batch Ozonation Experiments. The synthetic waters for batch experiments were prepared by decarbonating DDI water with scientific-grade nitrogen for 30 min at 20 °C followed by adding predetermined amounts of 0.1 M NaH_2PO_4, Na_2HPO_4, and $NaHCO_3$ stock solutions to achieve the target pH and total carbonate concentration, $C_{T,CO_3} = [H_2CO_3^*] + [HCO_3^-] + [CO_3^{2-}]$. After brief mixing, the solution was quickly transferred to a batch reactor. The batch ozone reactor was designed to prevent contact of the solution with the atmosphere during the experiments (Figure 1a). Ozone gas, produced from pure oxygen with an ozone generator model GL-1 (PCI Ozone and Control Systems, West Caldwell, NJ), was bubbled through DDI water of pH 5 (adjusted by adding H_2SO_4) in a 500-mL gas-washing cylinder to produce a stock solution of desired dissolved ozone concentration. Batch ozonation was initiated by transferring a predetermined volume of the stock solution into a 100-mL gas-tight syringe (SGE, Ringwood, Australia) holding a synthetic solution containing all other reactants and buffer chemicals. Dilution of the experimental water by addition of ozone stock solution was measured to be 9.7%. The concentration of each chemical species ($C_{T,CO_3} = 10^{-4}$ to 10^{-3} M, $C_{T,PO_4} = 10^{-3}$ M, $C_{T,0} = 0$−300 μg/L) and pH (6.5−8.5) presented in subsequent sections are those attained after dilution. Samples for ozone and bromate analyses were collected with 1- and 5-mL gas-tight syringes, respectively. Dissolved ozone present in each bromate sample of 5 mL was quenched with 0.1 mL of 0.05 M ethylenediamine solution immediately upon collection. Precautions were taken to minimize ozone volatilization during sample collection and processing. The temperature was controlled at 20 °C by immersing the syringe batch reactor in a water bath. All apparatus components that were in contact with ozone were made of glass, Teflon, or 316 stainless steel.

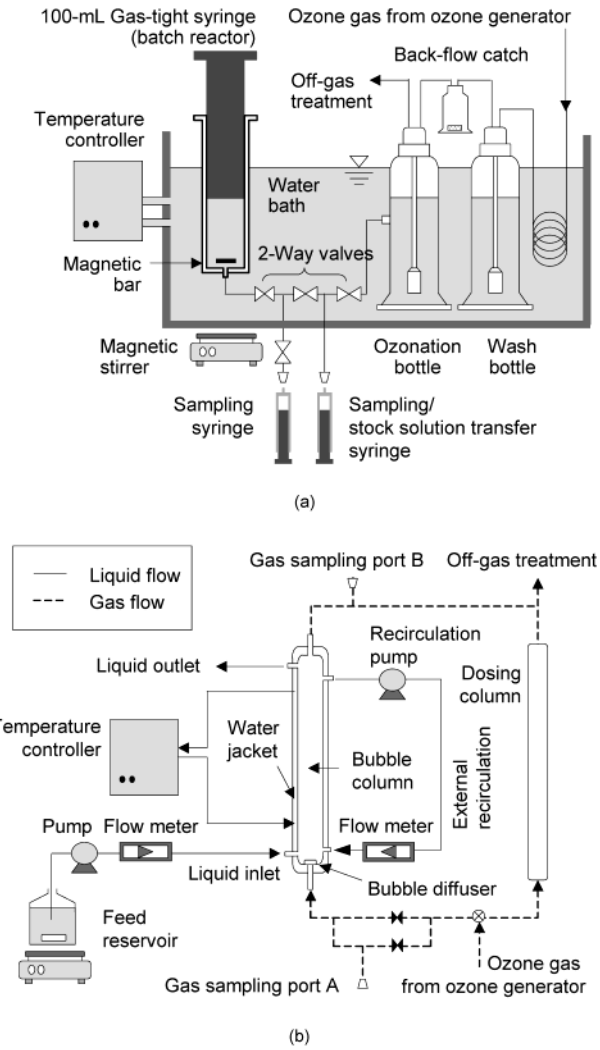

FIGURE 1. Schematics of lab-scale apparatus used for (a) batch ozonation and (b) flow-through ozonation experiments.

Semi-Batch Inactivation Experiments. The inactivation kinetics of *C. parvum* oocysts with ozone was determined with a semi-batch reactor in which the dissolved ozone concentration and temperature were kept constant at 0.5 ± 0.1 mg/L and 20 °C, respectively. A 200-mL volume of 0.01 M phosphate-buffered DDI water with pH adjusted to a target value of 6.5, 7.5, or 8.5 was used for all semi-batch tests. The procedures used for the *C. parvum* oocyst inactivation experiments were described in an earlier study (*2*). Samples were stored in 0.01% (v/v) Tween 20 solution at 4 °C, and viability was assessed within 48 h following the procedure described in a subsequent section.

Flow-Through Reactor Experiments. The flow-through ozone contactor (Figure 1b) consisted of a bubble column and a recirculation line. The bubble column was a glass tube with a length of 1.2 m and an i.d. of 21 mm, and the

recirculation line was a Teflon tube with an i.d. of 3/8 in. The volumes of the bubble column and the recirculation line were measured to be 440 and 85 mL, respectively. A feed reservoir was filled with 10^{-3} M phosphate-buffered solution in DDI water at pH 6.5, 7.5, or 8.5 and dosed with approximately 5×10^6 oocysts/L. A Masterflex model 7550-60 peristaltic pump (Cole-Parmer Instrument Co., Vernon Hills, IL) was used to introduce the feed solution into the bottom of the bubble column, which was operated in a co-current mode (i.e., both water and gas flowing upward). The applied feed flow rates were 17.5 or 34 mL/min, which corresponded to hydraulic residence times of 30.0 or 15.4 min, respectively. The water flowing through the bubble-diffuser column was externally recirculated from column outlet to inlet with a PTFE diaphragm pump (Cole-Parmer Instrument Co., Vernon Hills, IL) operated at a flow rate of 175 or 340 mL/min, which corresponded to a recirculation ratio (recirculation flow rate divided by feed flow rate) of $R = 10$ for both feed flow rates. Ozone gas produced from oxygen with the ozone generator model GL-1 (PCI Ozone and Control Systems, West Caldwell, NJ) was introduced at a flow rate of 60 mL/min through a glass-frit gas diffuser located at the bottom of the column. The temperature was kept constant at 20 °C with a surrounding water jacket that was connected to a temperature controller. All the tubing and reactor materials that were in contact with ozone were made of glass, Teflon, or 316 stainless steel.

Samples for dissolved ozone concentration measurement were collected directly from the liquid outlet of the bubble column with a gas-tight syringe. Samples with volumes of 20 and 500 mL were collected for bromate analysis and *C. parvum* oocyst viability assessment, respectively, after allowing the system to reach steady state (i.e., waiting approximately three times the hydraulic residence time under constant operating conditions). The sampling bottles contained sodium thiosulfate solution in excess and were continuously mixed to quench dissolved ozone in the sample upon collection. The oocysts were collected by passing the 500-mL sample through a Poretics Polycarbonate track-etched filter with a nominal pore size of 1.0 μm (Fisher Scientific, Itasca, IL) and resuspended in 0.01% (v/v) Tween 20 solution for storage at 4 °C. Oocyst viability was assessed within 48 h following the procedure described in a subsequent section. Different CT values were investigated by varying the ozone feed-gas concentration.

Tracer tests were performed using Rhodamine WT as the tracer compound to estimate the hydrodynamic conditions of the flow-through ozone contactor. The concentration of Rhodamine WT was determined with an Aminco Bowman series 2 spectrofluorometer (Rochester, NY) using excitation and emission wavelengths of 555 and 580 nm, respectively. Separate tracer tests were performed on the bubble column and recirculation line at the liquid flow rates of 18 and 182 mL/min, respectively. A mass of tracer was injected as a pulse input into the inlet of the bubble column or the recirculation line after allowing the system to reach a steady state. Oxygen gas was introduced into the bubble column at a flow rate of 60 mL/min with the power to the ozone generator turned off to avoid the oxidation of Rhodamine WT by ozone. Effluent samples of 2 mL were collected at maximum time intervals of 5 s for an overall period of at least 5 times the hydraulic residence time of each reactor component.

Analytical Methods. Aqueous and gaseous phase ozone concentrations were measured by a modified version (*40*) of the indigo colorimetric method (*41*). Bromate concentration was determined by conductivity detection with a DX-300 ion chromatography system (analytical column: IonPac AS9-HC; guard column: IonPac AG9-HC; eluent composition: 9 mM Na_2CO_3; eluent flow rate: 1.0 mL/min; sample loop size: 500 μL; detector: Dionex PED-2 pulsed electrochemical detector in conductivity mode) (Dionex Corporation, Sunnyvale, CA) (detection limit = 5 μg/L). The viability of *C. parvum* oocysts was determined by the modified in vitro excystation method (*2*).

Computer Simulations. A system of time-dependent first-order nonlinear ordinary differential equations with initial conditions was obtained by mathematically formulating chemical reactions in a batch system. The resulting system of equations was solved based on a semi-implicit method developed for ordinary differential equations that exhibit a stiffness problem (*42*). This solver algorithm was combined with the routines that provide an adaptive step size control over the period of integration in order to achieve desired accuracy with minimal computational effort. The library algorithms in C language were adopted from Press et al. (*43*) and modified and encoded for C/C++ programming language.

Results and Discussion

Mechanistic Model for Batch Ozone Reactor. Chemical reactions selected for mechanistic representation of ozone decomposition and bromate formation are summarized in Table 1. The overall bromate formation mechanism consists of three categories of reactions: (i) reactions responsible for ozone self-decomposition and corresponding production of secondary oxidants such as hydroxyl radical; (ii) reactions leading to the formation of bromate from bromide; (iii) reactions involving carbonate and phosphate species. In general, the chemical reactions and the corresponding rate constants were adopted as presented in the original study. The rate expressions for each species involved in the reactions shown in Table 1 were solved simultaneously to predict the ozone decomposition and bromate formation in a batch reactor.

Ozone Decomposition in Batch Ozone Reactor. Figure 2 shows the results for ozonation experiments with synthetic waters at pH 6.5, 7.5, and 8.5, and $C_{T,CO_3} = 10^{-3}$ M (a) and 10^{-4} M (b). Because the decomposition of ozone is initiated by hydroxide ion through reaction R1 or R1′ (Table 1) and propagates through radical reactions R5−R8 with hydroxyl radicals being scavenged by carbonate species according to reactions R52 and R53, it proceeds faster at higher pH and lower C_{T,CO_3}. The reactions R1 and R1′ have been proposed as an initiation step for ozone decomposition by Staehelin and Hoigné (*21*) and Forni et al. (*22*), respectively. The products of R1 are perhydroxyl ($HO_2^{\bullet}$) and superoxide ($O_2^{\bullet -}$) radicals, which directly induce the decomposition of ozone through the series of reactions R5−R8. The reactive product of R1′ is hydrogen peroxide, which initiates the ozone decomposition through reaction R3. Both R1 and R1′ have been used in various modeling studies due to the lack of clear experimental evidence to select one over the other. The experimental data were predicted well by the model with either R1 with the rate constant of 38 M^{-1} s^{-1} measured by Forni et al. (*22*) or R1′ with the rate constant of 70 M^{-1} s^{-1} used by Staehelin and Hoigné (*21*). Therefore, comparing model prediction only with ozone decomposition data did not provide decisive information to support the selection of either R1 or R1′. It is worthwhile to note that, in previous modeling studies, either of these initiation reactions has been used with corresponding rate constants being modified to fit the experimental ozone decomposition data (*68*−*71*). Such an approach was rejected for the present study because discrepancies between data and model predictions might have resulted from inaccuracies in not just one but actually several of many constants used in the model (e.g., inaccuracies in the rate constants of reactions R1−R15 were reported to range from 10 to 20%).

Using the reaction R1 or R1′ in the model, however, resulted in different levels of predicted hydroxyl radical

TABLE 1. Reactions and Corresponding Rate or Equilibrium Constants for Ozone Decomposition and Bromate Formation in Synthetic Water

no.	reaction	constant	ref	no.	reaction	constant	ref
			Ozone Decomposition				
R1	$O_3 + OH^- \rightarrow HO_2^\bullet + O_2^{\bullet-}$	$k_1 = 38\ M^{-1}\,s^{-1}$	*21*, *22*	R8	$HO^\bullet + O_3 \rightarrow HO_2^\bullet + O_2$	$k_8 = 2.6 \times 10^8\ M^{-1}\,s^{-1}$	*24*[c], *44*[c]
R1′	$O_3 + OH^- \rightarrow HO_2^- + O_2$	$k_1 = 70\ M^{-1}\,s^{-1}$	*21*, *22*	R8′	$HO^\bullet + O_3 \rightarrow HO_4^\bullet$	$k_{8'} = 2.0 \times 10^9\ M^{-1}\,s^{-1}$	*24*[e]
R2	$H_2O_2 \leftrightarrow HO_2^- + H^+$	$pK_a = 11.6$	*60*	R9	$HO^\bullet + H_2O_2 \rightarrow HO_2^\bullet + H_2O$	$k_9 = 2.7 \times 10^7\ M^{-1}\,s^{-1}$	*45*
R3	$O_3 + HO_2^- \rightarrow HO^\bullet + O_2^{\bullet-} + O_2$	$k_3 = 2.8 \times 10^6\ M^{-1}\,s^{-1}$	*21*[a]	R10	$HO^\bullet + HO_2^- \rightarrow O_2^{\bullet-} + H_2O$	$k_{10} = 7.5 \times 10^9\ M^{-1}\,s^{-1}$	*45*
R4	$HO_2^\bullet \leftrightarrow O_2^{\bullet-} + H^+$	$pK_a = 4.8$	*25*	R11	$HO^\bullet + HO^\bullet \rightarrow H_2O_2$	$k_{11} = 5.5 \times 10^9\ M^{-1}\,s^{-1}$	*24*
R5	$O_3 + O_2^{\bullet-} \rightarrow O_3^{\bullet-} + O_2$	$k_5 = 1.6 \times 10^9\ M^{-1}\,s^{-1}$	*25*[b], *43*[c]	R12	$HO^\cdot + O_2^{\bullet-} \rightarrow OH^- + O_2$	$k_{12} = 1 \times 10^{10}\ M^{-1}\,s^{-1}$	*24*
R6a	$O_3^{\bullet-} + H^+ \rightarrow HO_3^\bullet$	$k_{6a} = 5.2 \times 10^{10}\ M^{-1}\,s^{-1}$	*25*	R13	$HO^\bullet + HO_3^\bullet \rightarrow H_2O_2 + O_2$	$k_{13} = 5 \times 10^9\ M^{-1}\,s^{-1}$	*24*
R6b	$HO_3^\bullet \rightarrow O_3^{\bullet-} + H^+$	$k_{6b} = 3.3 \times 10^2\ s^{-1}$	*25*	R14	$O_2^{\bullet-} + HO_3^\bullet \rightarrow OH^- + 2O_2$	$k_{14} = 1 \times 10^{10}\ M^{-1}\,s^{-1}$	*24*
R7	$HO_3^\bullet \rightarrow HO^\bullet + O_2$	$k_7 = 1.1 \times 10^5\ s^{-1}$	*25*[d]	R15	$HO_3^\bullet + HO_3^\bullet \rightarrow H_2O_2 + 2O_2$	$k_{15} = 5 \times 10^9\ M^{-1}\,s^{-1}$	*24*
			Bromate Formation				
R20	$Br^- + O_3 \rightarrow O_2 + OBr^-$	$k_{20} = 160\ M^{-1}\,s^{-1}$	*46*	R31b	$HOBr + H^+ + Br^- \rightarrow Br_2 + H_2O$	$k_{31b} = 1.6 \times 10^{10}\ M^{-2}s^{-1}$	*53*
R21	$OBr^- + O_3 \rightarrow 2O_2 + Br^-$	$k_{21} = 330\ M^{-1}\,s^{-1}$	*46*	R32	$HOBr \leftrightarrow BrO^- + H^+$	$pK_a = 8.8$	*46*
R22	$OBr^- + O_3 \rightarrow BrO_2^- + O_2$	$k_{22} = 100\ M^{-1}\,s^{-1}$	*46*	R33	$OBr^- + Br^\bullet \rightarrow BrO^\bullet + Br^-$	$k_{33} = 4.1 \times 10^9\ M^{-1}\,s^{-1}$	*49*
R23	$BrO_2^- + O_3 \rightarrow BrO_3^- + O_2$	$k_{23} = 5.7 \times 10^4\ M^{-1}\,s^{-1}$	*46*, *47*[f]	R34	$OBr^- + {}^\bullet OH \rightarrow BrO^\bullet + OH^-$	$k_{34} = 4.2 \times 10^9\ M^{-1}\,s^{-1}$	*54*
R24a	$Br^- + {}^\bullet OH \rightarrow BrOH^{\bullet-}$	$k_{24a} = 1.1 \times 10^{10}\ M^{-1}\,s^{-1}$	*48*	R35	$HOBr + {}^\bullet OH \rightarrow BrO^\bullet + H_2O$	$k_{35} = 2.0 \times 10^9\ M^{-1}\,s^{-1}$	*49*
R24b	$BrOH^{\bullet-} \rightarrow Br^- + {}^\bullet OH$	$k_{24b} = 3.3 \times 10^7\ s^{-1}$	*48*	R36	$HOBr + O_2^{\bullet-} \rightarrow O_2 + Br^\bullet + OH^-$	$k_{36} = 3.5 \times 10^9\ M^{-1}\,s^{-1}$	*55*
R25a	$BrOH^{\bullet-} \rightarrow Br^\bullet + OH^-$	$k_{25a} = 4.2 \times 10^6\ s^{-1}$	*48*	R37	$HOBr + HO_2^- \rightarrow Br^- + O_2 + H_2O$	$k_{37} = 7.6 \times 10^8\ M^{-1}\,s^{-1}$	*56*
R25b	$Br^\bullet + OH^- \rightarrow BrOH^{\bullet-}$	$k_{25b} = 1.3 \times 10^{10}\ M^{-1}\,s^{-1}$	*49*	R38	$O_3 + Br^\bullet \rightarrow O_2 + BrO^\bullet$	$k_{38} = 1.5 \times 10^8\ M^{-1}\,s^{-1}$	*19*
R26	$BrOH^{\bullet-} + H^+ \rightarrow Br^\bullet + H_2O$	$k_{26} = 4.4 \times 10^{10}\ M^{-1}\,s^{-1}$	*48*	R39	$2BrO^\bullet + H_2O \rightarrow OBr^- + BrO_2^- + 2H^+$	$k_{39} = 5 \times 10^9\ M^{-1}\,s^{-1}$	*54*
R27	$BrOH^{\bullet-} + Br^- \rightarrow Br_2^{\bullet-} + OH^-$	$k_{27} = 2 \times 10^8\ M^{-1}\,s^{-1}$	*50*	R40	$BrO_2^- + BrO^\bullet \rightarrow OBr^- + BrO_2^\bullet$	$k_{40} = 4.0 \times 10^8\ M^{-1}\,s^{-1}$	*57*
R28a	$Br^\bullet + Br^- \rightarrow Br_2^{\bullet-}$	$k_{28a} = 1 \times 10^{10}\ M^{-1}\,s^{-1}$	*48*	R41	$BrO_2^- + {}^\bullet OH \rightarrow BrO_2^\bullet + OH^-$	$k_{41} = 2.0 \times 10^9\ M^{-1}\,s^{-1}$	*58*
R28b	$Br_2^{\bullet-} \rightarrow Br^\bullet + Br^-$	$k_{28b} = 1 \times 10^5\ s^{-1}$	*48*	R42	$BrO_2^- + Br_2^{\bullet-} \rightarrow OBr^- + BrO^\bullet + Br^-$	$k_{42} = 8 \times 10^7\ M^{-1}\,s^{-1}$	*54*
R29	$Br_2^{\bullet-} + Br_2^{\bullet-} \rightarrow Br_3^- + Br^-$	$k_{29} = 2 \times 10^9\ M^{-1}\,s^{-1}$	*51*	R43	$BrO_2^\bullet + {}^\bullet OH \rightarrow BrO_3^- + H^+$	$k_{43} = 2 \times 10^9\ M^{-1}\,s^{-1}$	*59*
R30a	$Br_3^- \rightarrow Br_2 + Br^-$	$k_{30a} = 8.3 \times 10^8\ s^{-1}$	*52*	R44a	$BrO_2^\bullet + BrO_2^\bullet \rightarrow Br_2O_4$	$k_{44a} = 6.0 \times 10^9\ M^{-1}\,s^{-1}$	*59*
R30b	$Br_2 + Br^- \rightarrow Br_3^-$	$k_{30b} = 10^{10}\ M^{-1}\,s^{-1}$	*52*	R44b	$Br_2O_4 \rightarrow BrO_2^\bullet + BrO_2^\bullet$	$k_{44b} = 3.1 \times 10^5\ s^{-1}$	*59*
R31a	$Br_2 + H_2O \rightarrow HOBr + H^+ + Br^-$	$k_{31a} = 97\ s^{-1}$	*53*	R45	$Br_2O_4 + OH^- \rightarrow BrO_3^- + BrO_2^- + H^+$	$k_{45} = 7 \times 10^8\ M^{-1}\,s^{-1}$	*54*
			Carbonate and Phosphate				
R50	$H_2CO_3{}^* \leftrightarrow H^+ + HCO_3^-$	$pK_{a,1} = 6.38$	*60*	R58	$CO_3^{\bullet-} + O_2^{\bullet-} \rightarrow CO_3^{2-} + O_2$	$k_{58} = 6.5 \times 10^8\ M^{-1}\,s^{-1}$	*64*[c], *65*[b]
R51	$HCO_3^- \leftrightarrow H^+ + CO_3^{2-}$	$pK_{a,2} = 10.38$	*60*	R59	$CO_3^{\bullet-} + HO_2^- \rightarrow CO_3^{2-} + HO_2^\bullet$	$k_{59} = 5.6 \times 10^7\ M^{-1}\,s^{-1}$	*64*
R52	$HO^\bullet + HCO_3^- \rightarrow HCO_3^\bullet + OH^-$	$k_{52} = 8.5 \times 10^6\ M^{-1}\,s^{-1}$	*61*	R60	$CO_3^{\bullet-} + H_2O_2 \rightarrow HCO_3^- + HO_2^\bullet$	$k_{60} = 8 \times 10^5\ M^{-1}\,s^{-1}$	*64*
R53	$HO^\bullet + CO_3^{2-} \rightarrow CO_3^{\bullet-} + OH^-$	$k_{53} = 3.9 \times 10^8\ M^{-1}\,s^{-1}$	*58*	R61	$H_3PO_4 \leftrightarrow H_2PO_4^- + H^+$	$pK_a = 2.3$	*60*
R54	$HCO_3^\bullet \leftrightarrow H^+ + CO_3^{\bullet-}$	$pK_a < 0$	*62*	R62	$H_2PO_4^- \leftrightarrow HPO_4^{2-} + H^+$	$pK_a = 7.2$	*60*
R55	$OBr^- + CO_3^{\bullet-} \rightarrow BrO^\bullet + CO_3^{2-}$	$k_{55} = 4.3 \times 10^7\ M^{-1}\,s^{-1}$	*54*	R63	$HPO_4^{2-} \leftrightarrow PO_4^{3-} + H^+$	$pK_a = 12.3$	*60*
R56	$BrO_2^- + CO_3^{\bullet-} \rightarrow BrO_2^\bullet + CO_3^{2-}$	$k_{56} = 1.1 \times 10^8\ M^{-1}\,s^{-1}$	*54*	R64	$O_3^{\bullet-} + H_2PO_4^- \rightarrow HO_3^\bullet + HPO_4^{2-}$	$k_{64} = 2.1 \times 10^8\ M^{-1}\,s^{-1}$	*25*
R57	$CO_3^{\bullet-} + O_3^{\bullet-} \rightarrow CO_3^{2-} + O_3$	$k_{57} = 6 \times 10^7\ M^{-1}\,s^{-1}$	*63*	R65	$HO_3^\bullet + HPO_4^{2-} \rightarrow O_3^{\bullet-} + H_2PO_4^-$	$k_{65} = 2.0 \times 10^7\ M^{-1}\,s^{-1}$	*25*
			Water				
R90	$H_2O \leftrightarrow H^+ + OH^-$	$pK_w = 14.17$	*60*				

[a] R3 was chosen over the reaction pathway of $O_3 + HO_2^- \rightarrow O_3^{\bullet-} + HO_2^\bullet$ proposed by ref *22* since R3 is kinetically more plausible. [b] From which rate constant for the same reaction was adopted. [c] From which reaction mechanism was adopted. [d] Different pathyway for ozonide radical decomposition involving oxygen atom radical ($O^{\bullet-}$) has been proposed by refs *22* and *23* but not included in this study since $O^{\bullet-}$ is negligible in neutral pH values. [e] This reaction and subsequent reactions involving $HO_4^\bullet$ were not included due to lack of sufficient evidence for the existence of this species. [f] Reported rate constant $BrO_2^- + O_3$ but proposed different products. Using the reaction $BrO_2^- + O_3 \rightarrow BrO_2^\bullet + O_3^{\bullet-}$ from this work resulted in significant overprediction of bromate formation for the conditions shown in Figures 5 and 6.

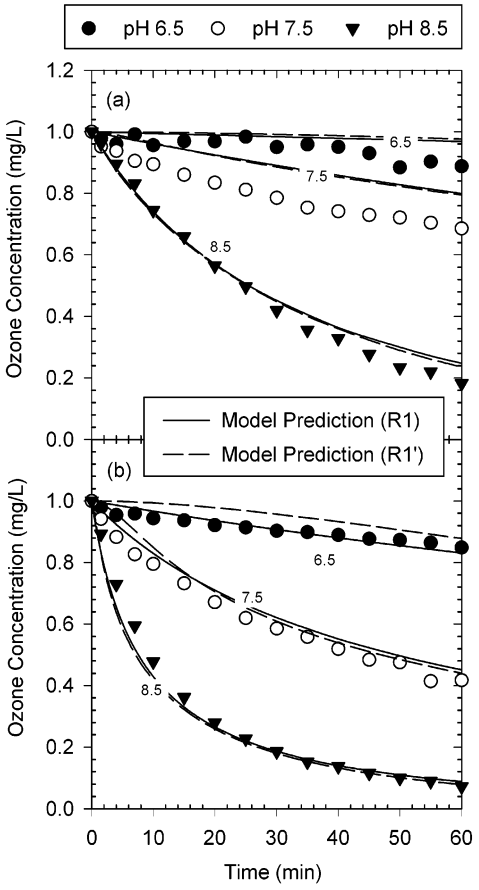

FIGURE 2. Comparison of ozone decomposition in batch ozone reactor measured experimentally and predicted with model at different pH and C_{T,CO_3} ($C_{O_3,0}$ = 1 mg/L; $C_{Br,0}$ = 0 mg/L; $C_{T,CO_3} = 10^{-3}$ M for (a) and 10^{-4} M for (b); $C_{T,PO_4} = 10^{-3}$ M; T = 20 °C).

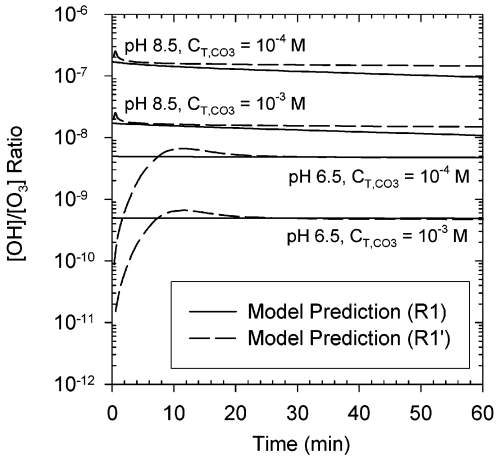

FIGURE 3. Model simulation of hydroxyl radical to ozone ratio during batch ozonation of synthetic waters.

concentrations. Figure 3 shows the model simulation of [•OH]/[O_3] ratio during ozone decomposition for the same experimental conditions given in Figure 2. As carbonate concentration decreased and pH increased, the [•OH]/[O_3] ratio increased due to reduced radical scavenging capacity and faster ozone decomposition into secondary oxidants. Employing different initiation steps resulted in similar [•OH]/[O_3] ratios at the later stage of ozonation, while model prediction with reaction R1′ showed an induction period of 2−20 min for reaching a plateau value. This period resulted from a gradual buildup of HO_2^- through reaction R3 followed by a delayed production of •OH. As also depicted in Figure 3, using R1′ in the model resulted in a curve having a point of inflection (concave down to concave up) at the initial stage of ozone decomposition especially at lower pH (e.g., pH 6.5, $C_{T,CO_3} = 10^{-4}$ M curve in Figure 2b). Additional model simulations showed that such a phenomenon became more pronounced when carbonate concentration was further decreased. Such an effect was also associated with the delay in overall ozone decomposition due to the time required for a buildup of sufficient HO_2^- especially at low pH. The model simulations in Figure 3, especially the one with R1 as the initiation reaction, were in good agreement with experimental data of Elovitz and von Gunten (*70*). Theses authors observed that the [•OH]/[O_3] ratio, defined as R_{ct} in their work, was approximately constant, independent of reaction time. R_{ct} was experimentally measured to be on the order of 10^{-8} at pH 8 and $C_{T,CO_3} = 2.6 \times 10^{-3}$ M in the presence of 70 μM methanol, a model promotor for the ozone−•OH transformation process, by using the hydroxyl radical probe, *p*-chlorobenzoic acid. Our model calculation, including the reactions involving methanol and *p*-chlorobenzoic acid, predicted R_{ct} values that were 1.6×10^{-8} initially and decreased to 8.0×10^{-9} after 30 min of reaction time. Consequently, the model developed in this study appears to be suitable to describe both ozone decomposition and •OH formation.

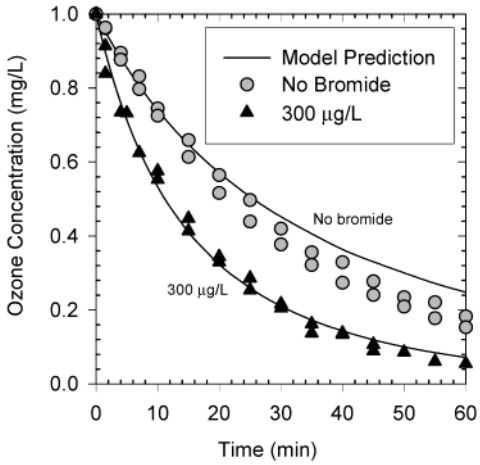

FIGURE 4. Effect of the presence of bromide ion on the decomposition of ozone in synthetic waters (pH 8.5; $C_{O_3,0}$ = 1 mg/L; $C_{T,CO_3} = 10^{-3}$ M; $C_{T,PO_4} = 10^{-3}$ M; T = 20 °C). Notice that duplicate data sets are presented for each condition and that one of the two data sets for the case of no-bromide has been adopted from Figure 2a.

The presence of bromide in water can have an effect on ozone decrease as illustrated in Figure 4. The decrease in ozone concentration in the presence of 300 μg/L proceeded at a faster rate as compared to that obtained in the absence of bromide (notice that the no-bromide curves shown in Figure 4 include the data presented in Figure 2a for pH 8.5 and a replicate curve). Similar to the observations discussed previously for experiments performed in the absence of bromide (Figure 2), model predictions with either R1 or R1′ (the latter not shown) were comparable to each other and in good agreement with experimental data. The greater ozone concentration decrease rate in the presence of bromide ion could be attributed to the reaction of ozone with various bromine species (reactions R20−R23 in Table 1). The main effect of bromide is the direct consumption of ozone through reaction R20. The other reactions have a relatively minor effect. Because of good reproducibility obtained for replicate ozone decomposition experiments in the presence of bromide, as illustrated with the duplicate curves shown in Figure 4, batch experiments for bromate formation presented in subsequent sections were performed without duplicating ozone concentration decrease curves.

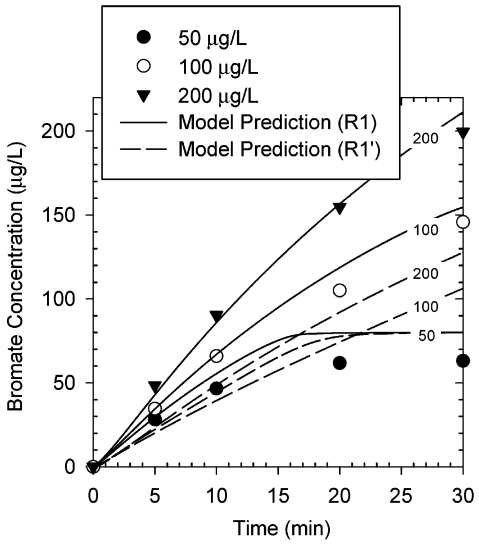

FIGURE 5. Comparison of bromate formation in batch ozone reactor measured experimentally and predicted with model at various initial bromide concentrations (pH 7.5; $C_{O_3,0} = 3.1$ mg/L; $C_{T,PO_4} = 10^{-3}$ M; $C_{T,CO_3} = 1.85 \times 10^{-4}$ M; $T = 20$ °C).

Bromate Formation in a Batch Ozone Reactor. Results for bromate formation experiments at different initial bromide concentrations and pH 7.5 and corresponding model predictions are shown in Figure 5. Bromate formation predictions using either R1 or R1′ as the initiation reaction for the initial bromide concentration of 50 μg/L were comparable and in good agreement with the corresponding experimental data. The agreement between predicted and experimental curves was considered satisfactory based on the fact that, as pointed out in a previous section, the chemical reactions and corresponding rate constants were adopted as presented in a multitude of original studies.

In contrast to the observation at the lowest bromide concentration tested, greater discrepancy was observed between model predictions with reactions R1 and R1′ at the two higher bromide ion concentrations of 100 and 200 μg/L investigated (Figure 5). Furthermore, using initiation reaction R1′ resulted in significant underestimation of bromate formation, with the level of discrepancy being more marked at higher bromide concentration as depicted in Figure 5. In contrast, model predictions with reaction R1 were in good agreement with experimental results.

The effect of initial bromide concentration on bromate formation at pH 8.5 is depicted in Figure 6. Similar to the observation at pH 7.5 (Figure 5), bromate formation predictions using either R1 or R1′ were comparable and in reasonably good agreement with the corresponding experimental data at the lowest initial bromide concentration of 100 μg/L investigated at pH 8.5. Also similar to the observation at pH 7.5, the use of initiation reaction R1′ resulted in significant underprediction of bromate formation at pH 8.5, and the deviation was once again more pronounced at higher initial bromide concentration within the range investigated. Furthermore, contrary to the trends observed for the experimental data, the model with R1′ predicted a decrease in ultimate bromate formation with increasing initial bromide concentration. Model calculations with R1′ at either pH 7.5 or 8.5 revealed that, in the presence of relatively high levels of bromide, the reaction between HO_2^- and HOBr (reaction R37) prevented the initial buildup of the key intermediate HOBr/OBr^- pair for bromate formation. In other words, relatively high production of HO_2^- from reaction R1′ (i.e., HO_2^- concentrations predicted with the model using reaction R1′ were in the range of 10^{-7}–10^{-9} M for the conditions shown

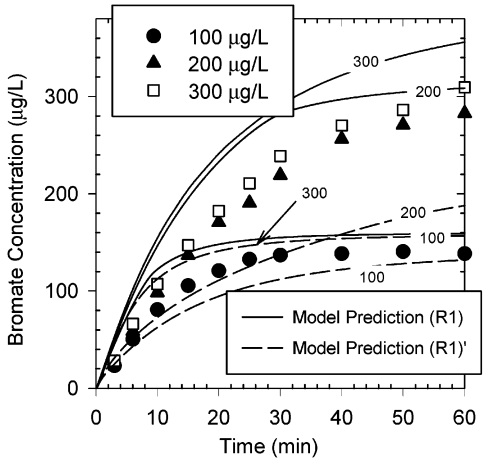

FIGURE 6. Comparison of bromate formation in batch ozone reactor measured experimentally and predicted with model at various initial bromide concentrations (pH 8.5; $C_{O_3,0} = 1.0$ mg/L; $C_{T,PO_4} = 10^{-3}$ M; $C_{T,CO_3} = 10^{-3}$ M; $T = 20$ °C).

in Figures 5 and 6) was responsible for the underestimation in bromate formation. In contrast, the use of initiation reaction R1 provided better agreement with the trends observed for experimental results at pH 8.5, even though the formation of bromate was generally overestimated. Therefore, reaction R1 was selected for all model predictions presented subsequently.

Results for experiments performed to assess the effect of pH within the range of 6.3–8.0 on bromate formation are shown in Figure 7a. The model predicted experimental data reasonably well at the lowest pH of 6.3 investigated, but predictions deviated from the data at higher pH, with the discrepancies being more pronounced at longer reaction times. The results obtained for additional experiments performed to assess if similar deviations between predicted and experimental bromate formation would be observed at high pH (pH 8.5) for different initial dissolved ozone concentrations in the range of 0.5–1.5 mg/L are shown in Figure 8. As depicted in panel a, good agreement was observed between model prediction and experimental data at the lowest ozone dose (0.5 mg/L) used. In contrast, consistent with the observation at high pH levels and an ozone dose of 1.0 mg/L in Figure 7, the model overpredicted bromate formation at the higher ozone doses of 1.0 and 1.5 mg/L investigated. Although no definite explanation could be provided at this time for the occurrence of these discrepancies, they might have resulted, at least partially, from compounding errors associated with inaccuracies in some of the rate constant values listed in Table 1. For example, the rate constants for the oxidation of bromine species by ozone (reactions R20–R22, Table 1) have been reported to have average uncertainties of 17% (*48*). Although this variability was observed to affect the formation of bromate predicted by the model as illustrated with the dotted lines in Figure 7a, it could not solely explain the observed discrepancies. However, errors associated with some of the other rate constant values used could have compounded to account for at least a portion of the overall deviations observed. Unfortunately, uncertainties for many of the rate constants summarized in Table 1 have not been reported, and thus such more general analysis could not be performed at this time. Another potential explanation for the lower bromate formation observed experimentally as compared to model predictions could be the occurrence of reactions not accounted for in Table 1. One such reaction could be the scavenging of hydroxyl radicals by trace organic matter that is unavoidably present in DDI water and chemical reagents. However, additional model calculations (results not shown)

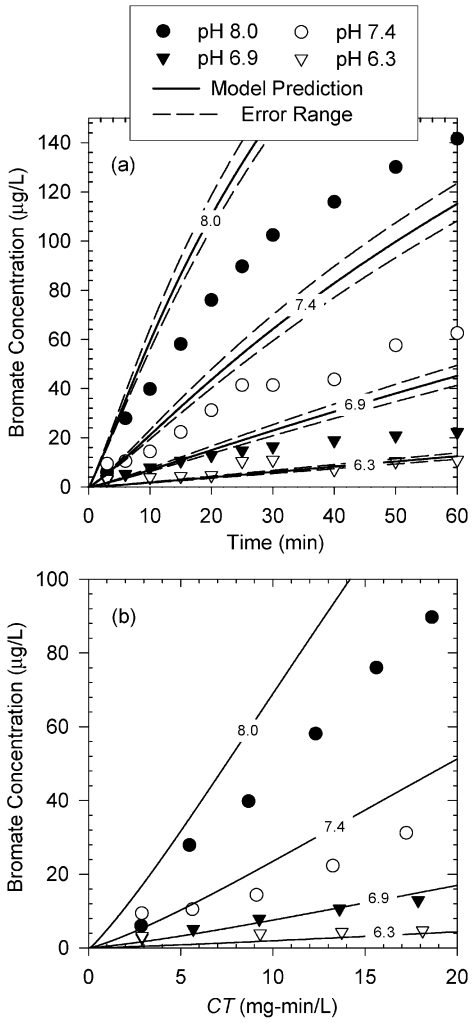

FIGURE 7. Comparison of bromate formation in batch ozone reactor measured experimentally and predicted with model at different pH levels ($C_{O_3,0}$ = 1.0 mg/L; $C_{Br,0}$ = 200 μg/L; C_{T,CO_3} = 10^{-3} M; C_{T,PO_4} = 10^{-3} M; T = 20 °C).

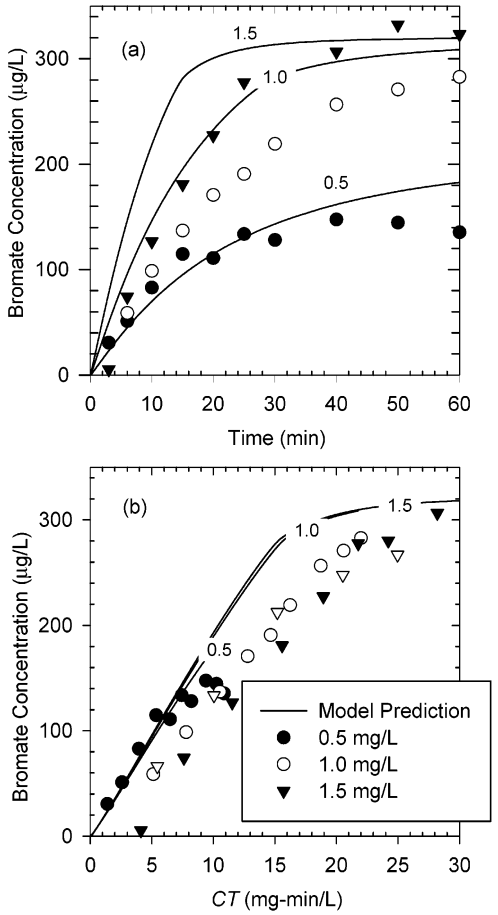

FIGURE 8. Comparison of bromate formation vs (a) time and (b) CT measured experimentally and predicted with model at different initial ozone doses (pH 8.5; $C_{Br,0}$ = 200 μg/L; C_{T,PO_4} = 10^{-3} M; C_{T,CO_3} = 10^{-3} M; T = 20 °C).

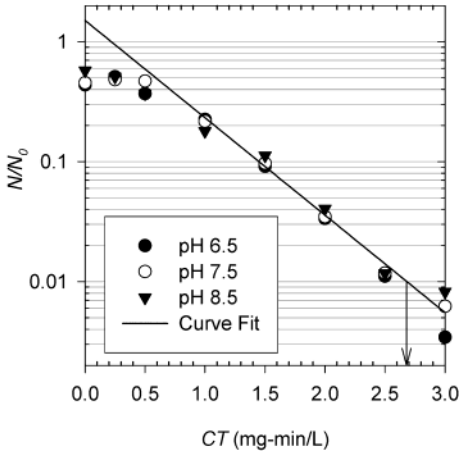

FIGURE 9. Inactivation kinetics of *C. parvum* oocysts (lot A) during semibatch ozonation (C_{T,PO_4} = 10 mM; T = 20 °C).

assuming dissolved organic carbon concentrations of up to 0.2 mg/L and typical hydroxyl radical scavenging rate constant values published elsewhere (*29*, *69*) revealed that such effect should be negligible for the experimental conditions used in Figures 7 and 8.

Bromate formation curves obtained from both experiments and model predictions had a tendency to merge into a single line when they were plotted versus CT (Figure 8b), a common independent variable used in disinfection. CT values were calculated by integrating the ozone concentration curve with respect to time. Although there are some deviations mainly with experimental data, the trends observed in both experiments and model predictions suggest that the CT-normalized bromate formation tends to be independent of the ozone dose used in a batch reactor. This observation is analogous to the CT concept for *C. parvum* oocyst inactivation (*4*). However, in contrast to the lack of pH effect reported for the inactivation kinetics of *C. parvum* oocysts with ozone (*4*), distinct curves, both experimental and predicted, were obtained when plotting the bromate data at different pH values versus CT as depicted in Figure 7b. Similarly, other water quality parameters (e.g., alkalinity, ammonia, dissolved organic carbon) could affect bromate formation without having an impact on *C. parvum* oocyst inactivation.

***C. parvum* Oocyst Inactivation Kinetics.** Results obtained for the semi-batch ozone disinfection experiments with *C. parvum* oocysts from lot A are presented in Figure 9. Similar results were obtained for lot B. Consistent with earlier observations (*4*), the inactivation curves for both lots A and B were found to be independent of pH when plotted versus CT. The inactivation kinetics was represented with the delayed pseudo-first-order Chick−Watson model: $N/N_0 = 1$ for CT < $\ln(N_1/N_0)/k_N$, and $N/N_0 = N_1/N_0 \exp(-k_N CT)$ for CT ≥ $\ln(N_1/N_0)/k_N$ (*72*). The lag-phase factors were N_1/N_0 = 1.50 and 3.72 (dimensionless), and the pseudo-first-order kinetic rate constants were k_N = 1.87 and 2.04 L mg^{-1} min^{-1} for oocysts from lots A and B, respectively. These kinetic

constants were used to predict *C. parvum* oocyst inactivation efficiencies with the flow-through reactor model.

Flow-Through Ozone Contactor Modeling. Tracer test results separately obtained for the bubble-diffuser column and the recirculation line were analyzed to determine dispersion numbers using the axial dispersion reactor model with the assumption of closed-vessel boundary conditions (*73*). The resulting dispersion number was 0.01 (i.e., Péclet number of 100) for both reactor components. This analysis revealed that each component of the bench-scale flow-through reactor behaved similar to an ideal plug-flow reactor (PFR). Therefore, the entire reactor was represented with a PFR-side PFR model. Notice that even though each of the two reactor components could be modeled separately as a PFR, the overall reactor behaved closer to a CSTR due to the relatively high recirculation ratio ($R = 10$) used. The mechanistic model for ozone decomposition and bromate formation was combined with additional mass balances for gaseous phase ozone as previously described (*34*). The overall volumetric mass transfer coefficients for specific operating conditions were estimated with an empirical correlation (*34, 73*). Average bubble size in the bubble-diffuser column, a critical parameter in the mass transfer correlation, was measured photographically. The model calculation along the bubble column and recirculation line was iterated with respect to time (i.e., hydraulic residence time of each compartment) using the batch ozone contactor model until sufficient convergence criteria were met at the inlet of the reactor. Preliminary model simulations showed that the dissolved ozone concentration along the depth of the bubble column was approximately uniform due to mixing by the external recirculation. Therefore, the CT values were calculated as a product of the predicted outlet dissolved ozone concentrations and hydraulic residence times. [CT in this study is based on hydraulic residence time and not on characteristic time t_{10} used in U.S. EPA regulations.] Finally, the level of *C. parvum* oocyst inactivation was estimated by calculating the exposure to dissolved ozone assuming uniform distribution of dissolved ozone throughout the bubble column and external recirculation line.

Simultaneous Prediction of Bromate Formation and *C. parvum* Oocyst Inactivation in the Flow-Through Ozone Reactor. Results obtained for experiments performed to investigate the effect of pH on bromate formation and *C. parvum* oocyst inactivation in the flow-through reactor are shown versus corresponding CT values in Figure 10a,b. The corresponding model predictions also shown in the figure represented the experimental data reasonably well. Consistent with the batch (Figure 7) and semi-batch (Figure 9) reactor observations, the formation of bromate was greatly affected by pH, while the inactivation of *C. parvum* oocysts was pH independent (Figure 10b).

Bromate formation and *C. parvum* oocyst inactivation results obtained at a constant pH of 7.5, and two different reactor inlet liquid flow rates of 34 and 17.5 mL/min, corresponding to an HRT of 15.4 and 30.0 min, respectively, are shown in Figure 10a,c. Experimental data as well as model predictions showed that the levels of bromate formation and *C. parvum* oocyst inactivation were dependent only on CT with flow rate having little effect within the range of conditions investigated. This observation was once again consistent with batch experimental results for bromate formation (Figure 8) and semi-batch data for *C. parvum* oocyst inactivation (Figure 9).

Additional model simulations were performed using the batch reactor model to compare the bromate formation and *C. parvum* oocyst inactivation that would take place in an ideal PFR to those determined in the PFR-side PFR flow-through reactor used in this study. As depicted in Figure 10a, the formation of bromate in the flow-through reactor did

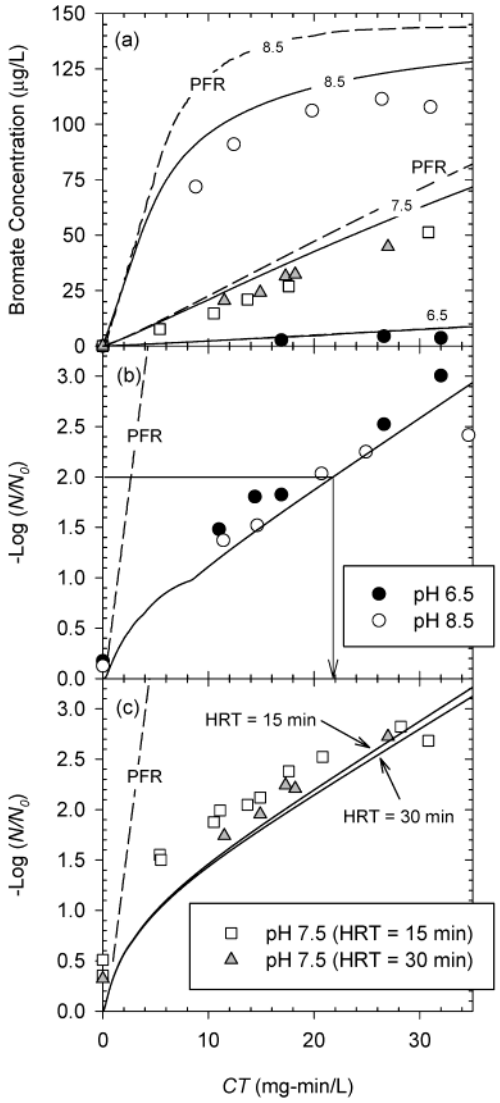

FIGURE 10. Comparison of (a) bromate formation and (b and c) *C. parvum* oocyst inactivation measured experimentally and predicted with model at different pH levels and operating conditions (*C. parvum* oocyst lot A for pH 6.5 and pH 8.5, lot B for pH 7.5; $C_{Br,0} = 90$ μg/L for pH 6.5 and pH 8.5; $C_{Br,0} = 100$ μg/L for pH 7.5; $C_{T,CO_3} = 2.95 \times 10^{-5}$ M for pH 6.5; $C_{T,CO_3} = 1.85 \times 10^{-4}$ M for pH 7.5; $C_{T,CO_3} = 1.80 \times 10^{-3}$ M for pH 8.5; $C_{T,PO_4} = 10^{-3}$ M; $T = 20$ °C). Continuous and dashed lines represent bromate formation and *C. parvum* oocyst inactivation predicted with PFR-side PFR and PFR models, respectively.

not deviate greatly from that predicted for a PFR. In contrast, as shown in Figure 10b,c, a great discrepancy was obtained between the inactivation efficiency of *C. parvum* oocysts in the flow-through reactor used in this study and that predicted for a PFR. This phenomenon resulted from the difference in the level of conversion associated to the formation of bromate from bromide as compared to that for the inactivation of *C. parvum* oocysts. Because *C. parvum* oocyst inactivation involved much higher conversion (e.g., 96−99.9% in Figure 10b,c) than bromate formation (e.g. less than 30% for all conditions in Figure 10a), deviations in reactor hydrodynamic conditions from ideal PFR had a much greater effect on *C. parvum* oocyst inactivation than on bromate formation. This was consistent with the observation in Figure 10a that bromate formation in the flow-through reactor deviated from that predicted for a PFR more at pH 8.5 than at lower pH values since conversion of bromide to bromate increased when pH increased. The impact of hydrodynamics on *C. parvum* oocyst inactivation was apparent when experimental

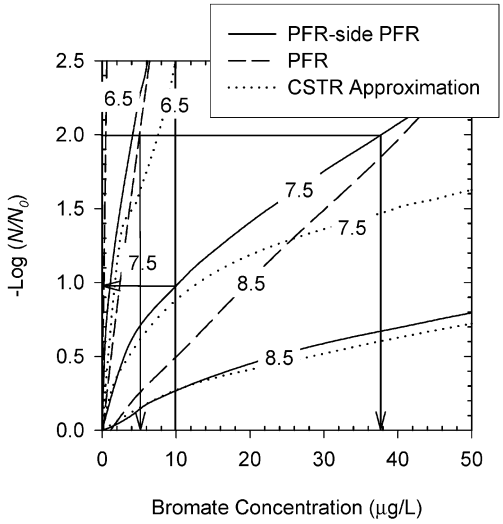

FIGURE 11. Simultaneous prediction of *C. parvum* oocyst inactivation and bromate formation in PFR-side PFR, PFR, and CSTR ozone contactors at different pH levels (*C. parvum* oocyst lot A; $C_{Br,0} = 100$ μg/L; $C_{T,CO_3} = 2.95 \times 10^{-5}$ M for pH 6.5; $C_{T,CO_3} = 1.85 \times 10^{-4}$ M for pH 7.5; $C_{T,CO_3} = 1.80 \times 10^{-3}$ M for pH 8.5; $C_{T,PO_4} = 10^{-3}$ M; $T = 20$ °C).

results with a semi-batch reactor were compared to those with a flow-through reactor. For example, the CT required to achieve an inactivation efficiency of 99% in the flow-through reactor of this study (~24 mg min L^{-1}, Figure 10b) was more than eight times greater than that in the semi-batch reactor (~2.7 mg min L^{-1}, Figure 9).

Model Application. *C. parvum* oocyst inactivation levels expected at different pH levels in the flow-through reactor used in this study (i.e., PFR-side PFR), an ideal PFR, and an ideal CSTR (approximated by PFR-side PFR with a high recirculation ratio of $R = 100$) are shown versus the levels of bromate formation expected at the same conditions in Figure 11. Model simulation suggests that bromate formation is much lower when the reactor mixing conditions are closer to PFR and farther from CSTR conditions for the same level of inactivation efficiency. For example, for a target *C. parvum* oocyst inactivation of 99% at pH 7.5, bromate formation in the PFR is expected to be 5 μg/L, which is significantly lower than 38 μg/L expected in the PFR-side PFR reactor and > 50 μg/L in the CSTR. Figure 11 also shows that the level of *C. parvum* oocyst inactivation in the PFR is much higher than those in the PFR-side PFR reactor and the CSTR for the same level of bromate formation. For example, when complying with the current drinking water standard of 10 μg/L for bromate formation, the level of *C. parvum* oocyst inactivation in the PFR is expected to be >99.9% at pH 7.5, which is much greater than about 90% expected for the reactor used in this study. When the reactor is closer to CSTR, even lower inactivation efficiency is expected. Therefore, the model simulation suggests that it is beneficial to design the ozone contactor closer to ideal PFR when simultaneous control of bromate formation and *C. parvum* oocyst inactivation is needed.

However, as shown in Figure 11 and consistent with previous observations, pH also has great impact on bromate formation. For example, an inactivation efficiency of 99% could be achieved with negligible bromate formation at pH 6.5, while a very large amount of bromate (≫50 μg/L) might be formed at pH > 7.5 for the same level of inactivation. Therefore, pH depression might be necessary even if the hydrodynamic conditions are close to PFR to achieve the simultaneous goals of bromate formation control and *C. parvum* oocyst inactivation.

It is important to point out that although the general trends depicted in Figure 11 are valid, absolute values for the concentration of bromate formed at a given level of *C. parvum* oocyst inactivation might not be accurate in view of the discrepancies observed between model predictions and experimental results observed for both batch and flow-through reactors under some of the conditions investigated.

Acknowledgments

This research was partially funded by the U.S. Environmental Protection Agency and the American Water Works Association Research Foundation. The authors acknowledge Mark Urban and Dr. Shinya Echigo for their assistance in laboratory work during their stay at the University of Illinois and Dr. Michael Elovitz and Dr. Roger Minear for fruitful discussions. The authors also extend their gratitude to Dr. Marilyn Marshall for providing information about *C. parvum* oocysts and to Dr. Gary Amy for providing the lab-scale flow-through ozone contactor. Experiments were performed at the William H. Richardson Memorial Disinfection Laboratory of the University of Illinois.

Supporting Information Available

Two figures. This material is available free of charge via the Internet at http://pubs.acs.org.

Literature Cited

(1) Gyürék, L. L.; Li, H.; Belosevic, M.; Finch, G. R. *J. Environ. Eng.* **1999**, *125*, 913−924.
(2) Rennecker, J. L.; Mariñas, B. J.; Rice, E. W.; Owens, J. H. *Water Res.* **1999**, *33*, 2481−2488.
(3) Rennecker, J. L.; Driedger, A. M.; Rubin, S. A.; Mariñas, B. J. *Water Res.* **2000**, *34*, 4121−4130.
(4) Rennecker, J. L.; Kim, J. H.; Corona-Vasquez, B.; Mariñas, B. J. *Environ. Sci. Technol.* **2001**, *35*, 2752−2757.
(5) Driedger, A. M.; Rennecker, J. L.; Mariñas, B. J. *Water. Res.* **2000**, *34*, 3591−3597.
(6) Driedger, A. M.; Rennecker, J. L.; Mariñas, B. J. *Water Res.* **2001**, *35*, 41−48.
(7) Gyürék, L.; Finch, G. R.; Belosevic, M. *J. Environ. Eng.* **1997**, *123*, 865−875.
(8) Glaze, W. H.; Weinberg, H. S.; Cavanagh, J. E. *J. Am. Water Works Assoc.* **1993**, *85*, 96−103.
(9) Krasner, S. W.; Glaze, W. H.; Weinberg, H. S.; Daniel, P. A.; Najm, I. S. *J. Am. Water Works Assoc.* **1993**, *85*, 73−81.
(10) Shukairy, H. M.; Miltner, R. J.; Summers, R. S. *J. Am. Water Works Assoc.* **1994**, *86*, 72−87.
(11) National Primary Drinking Water Regulations; Disinfectants and Disinfection Byproducts; Final Rule. *Fed. Regist.* **1998**, *63* (241), 69389.
(12) European Union. Amtsblatt der Europäischen Gemeinschaften. Richtlinie 98/83/EG des Rates. 3-12-1998; 1998, pp 32−54.
(13) Korich, D. G.; Mead, J. R.; Madore, M. S.; Sinclair, N. A.; Sterling, C. R. *J. Am. Water Works Assoc.* **1990**, *87*, 54−68.
(14) Siddiqui, M. S.; Amy, G. L. *J. Am. Water Works Assoc.* **1993**, *85*, 63−72.
(15) Siddiqui, M. S.; Amy, G. L.; Ozekin, K.; Westerhoff, P. *Ozone Sci. Eng.* **1994**, *16*, 157−178.
(16) Song, R.; Westerhoff, P.; Minear, R.; Amy, G. L. *J. Am. Water Works Assoc.* **1997**, *89*, 69−78.
(17) Yates, R. S.; Stenstrom, M. K. *Proc. Am. Water Works Assoc. Annu. Conf.* **1993**, 475−499.
(18) von Gunten, U.; Hoigné, J. *Environ. Sci. Technol.* **1994**, *28*, 1234−1242.
(19) von Gunten, U.; Oliveras, Y. *Environ. Sci. Technol.* **1998**, *32*, 63−70.
(20) Westerhoff, P.; Song, R.; Amy, G.; Minear, R. *Water Res.* **1998**, *32*, 1687−1699.
(21) Staehelin, J.; Hoigné, J. *Environ. Sci. Technol.* **1982**, *16*, 676−681.
(22) Forni, L.; Bahnemann, D.; Hart, E. J. *J. Phys. Chem.* **1982**, *86*, 255−259.
(23) Tomiyasu, H.; Fukutomi, H.; Gordon, G. *Inorg. Chem.* **1985**, *24*, 2962−2966.
(24) Staehelin, J.; Bühler, R. E.; Hoigné, J. *J. Phys. Chem*, **1984**, *88*, 5999−6004.

(25) Bühler, R. E.; Staehelin, J.; Hoigné, J. *J. Phys. Chem.* **1984**, *88*, 2560−2564.
(26) Pinkernell, U.; von Gunten, U. *Environ. Sci. Technol.* **2001**, *35*, 2525−2531.
(27) Hofmann, R.; Andrews, R. C. *Water Res.* **2001**, *35*, 599−604.
(28) Acero, J. L.; von Gunten, U. *Ozone Sci. Eng.* **2000**, *22*, 305−328.
(29) von Gunten, U. *Water Res.* **2003**, *37*, 1469−1487.
(30) Lev, O.; Regli, S. *J. Environ. Eng*, **1992**, *118*, 268−285.
(31) Smith, D. W.; Zhou, H. *Ozone Sci. Eng.* **1994**, *16*, 429−441.
(32) Kim, J. H.; Tomiak, R. B.; Rennecker, J. L.; Mariñas, B. J.; Miltner, R. J.; Owens, J. H. *J. Environ. Eng.* **2002**, *128*, 514−521.
(33) Kim, J. H.; Tomiak, R. B.; Mariñas, B. J. *J. Environ. Eng.* **2002**, *128*, 522−532.
(34) Gujer, W.; von Gunten, U. *Water Res.* **2003**, *37*, 1667−1677.
(35) Siddiqui, M. S.; Amy, G. L.; Ozekin, K.; Westerhoff, P. *Water, Air, Soil Pollut.* **1998**, *108*, 1−32.
(36) Roustan, M.; Duguet, J. P.; Lainé, J. M.; Do-Quang, Z.; Mallevialle, J. *Ozone Sci. Eng.* **1996**, *18*, 87−97.
(37) von Gunten, U.; Bruchet, A.; Costentin, E. *J. Am. Water Works Assoc.* **1996**, *88*, 53−65.
(38) von Gunten, U.; Pinkernell, U. *Water Sci. Technol.* **2000**, *41*, 53−59.
(39) Bellamy, W. D.; Damez, F.; Langlais, B.; Montiel, A.; Rakness, K. L.; Reckhow, D. A.; Robson, C. M. In *Ozone in Water Treatment Application and Engineering*; Langlais, B., Reckhow, D. A., Brink, D. R., Eds.; American Water Works Association Research Foundation: Denver, and Lewis Publishers: Chelsea, MI, 1991; Chapter IV.
(40) Chiou, C. F.; Mariñas, B. J.; Adams, J. Q. *Ozone Sci. Eng.* **1995**, *17*, 329−344.
(41) Bader, H.; Hoigné, J. *Water Res.* **1981**, *15*, 449−456.
(42) Bader, G.; Deuflhard, P. *Numer. Math.* **1983**, *41*, 373−398.
(43) Press, W. H.; Teukolsky, S. A.; Vetterling, W. T.; Flannery, B. P. *Numerical Recipes in C*, 2nd ed.; Cambridge University Press: New York, 1992.
(44) Kim, J. H. Integrated Optimization of Cryptosporidium Inactivation and Bromate Formation Control in Ozone Contactors. Ph.D. Dissertation, University of Illinois, 2002; pp 11−16 and 19−30.
(45) Sehested, K.; Holcman, J.; Hart, E. J. *J. Phys. Chem*, **1983**, *87*, 1951−1954.
(46) Sehested, K.; Holcman, J.; Bjergbakke, E.; Hart, E. J. *J. Phys. Chem*, **1984**, *88*, 4144−4147; **1985**, *89*, 388 (Addendum).
(47) Christensen, H.; Sehested, K.; Corfitzen, H. *J. Phys. Chem.* **1982**, *86*, 1588−1590.
(48) Haag, W. R.; Hoigné, J. *Environ. Sci. Technol.* **1983**, *17*, 261−267.
(49) Nicoson, J. S.; Wang, L.; Becker, R. H.; Huff Hartz, K. E.; Muller, C. E.; Margerum, D. W. *Inorg. Chem.* **2002**, *41*, 2975−2980.
(50) Zehavi, D.; Rabani, J. *J. Phys. Chem.* **1972**, *76*, 312−319.
(51) Kläning, U. K.; Wolff, T. *Ber. Bunsen-Ges. Phys. Chem.* **1985**, *89*, 243−245.
(52) Mamou, A.; Rabani, J.; Behar, D. *J. Phys. Chem*, **1977**, *81*, 1447−1448.
(53) Neta, P.; Huie, R. E.; Ross, A. B. *J. Phys. Chem. Ref. Data* **1988**, *17*, 1027−1284.
(54) Sidgwick, N. V. *The Chemical Elements and Their Compounds*: *Vol. II*; Oxford Press: Oxford, 1952.
(55) Beckwith, R. C.; Wang, T. X.; Margerum. D. W. *Inorg. Chem.* **1996**, *35*, 995−1000.
(56) Buxton, G. V.; Dainton, F. S. *Proc. R. Soc. London A* **1968**, *304*, 427−439.
(57) Schwarz, H. A.; Bielski, B. H. J. *J. Phys. Chem.* **1986**, *90*, 1445−1448.
(58) von Gunten, U.; Oliveras, Y. *Water Res.* **1997**, *31*, 900−906.
(59) Amichai, O.; Treinin, A. *J. Phys. Chem.* **1970**, *74*, 3670−3674.
(60) Buxton, G. V.; Greenstock, C. L.; Helman, W. P.; Ross, A. B. *J. Phys. Chem. Ref. Data* **1988**, *17*, 513−886.
(61) Field, R. J.; Raghavan, N. V.; Brummer, J. G. *J. Phys. Chem.* **1982**, *86*, 2443−2449.
(62) Snoeyink, V. L.; Jenkins, D. *Water Chemistry*; John Wiley & Sons: New York, 1980.
(63) Buxton, G. V.; Elliot, A. J. *Radiat. Phys. Chem.* **1986**, *27*, 241−243.
(64) Czapski, G.; Lymar, S. V.; Schwarz, H. A. *J. Phys. Chem*, **1999**, *103*, 3447−3450.
(65) Holcman, J.; Sehested, K.; Bjergbakke, E.; Hart, E. J. *J. Phys. Chem.* **1982**, *86*, 2069−2072.
(66) Behar, D.; Czapski, G.; Duchovny, I. *J. Phys. Chem.* **1970**, *74*, 2206−2210.
(67) Eriksen, T. E.; Lind, J.; Merenyi, G. *Radiat. Phys. Chem.* **1985**, *26*, 197−199.
(68) Chelkowska, K.; Grasso, D.; Fábián, I.; Gordon, G. *Ozone Sci. Eng.* **1992**, *14*, 33−49.
(69) Westerhoff, P.; Song, R.; Amy, G.; Minear, R. *Ozone Sci. Eng.* **1997**, *19*, 55−74.
(70) Elovitz, M. S.; von Gunten, U. *Ozone Sci. Eng.* **1999**, *21*, 239−260.
(71) Nemes, A.; Fábián, I.; Gordon, G. *Ozone Sci. Eng.* **2000**, *22*, 287−304.
(72) Wickramanayake, G. B.; Sproul, O. J. *Ozone Sci. Eng.* **1988**, *10*, 125−135.
(73) Mariñas, B. J.; Liang, S.; Aieta, M. E. *J. Am. Water Works Assoc.* **1993**, *85*, 90−99.

Received for review July 14, 2003. Revised manuscript received January 11, 2004. Accepted January 20, 2004.

ES034760W